Supporting information

Effect of PEG Grafting density on colloidal stability of AuNPs.

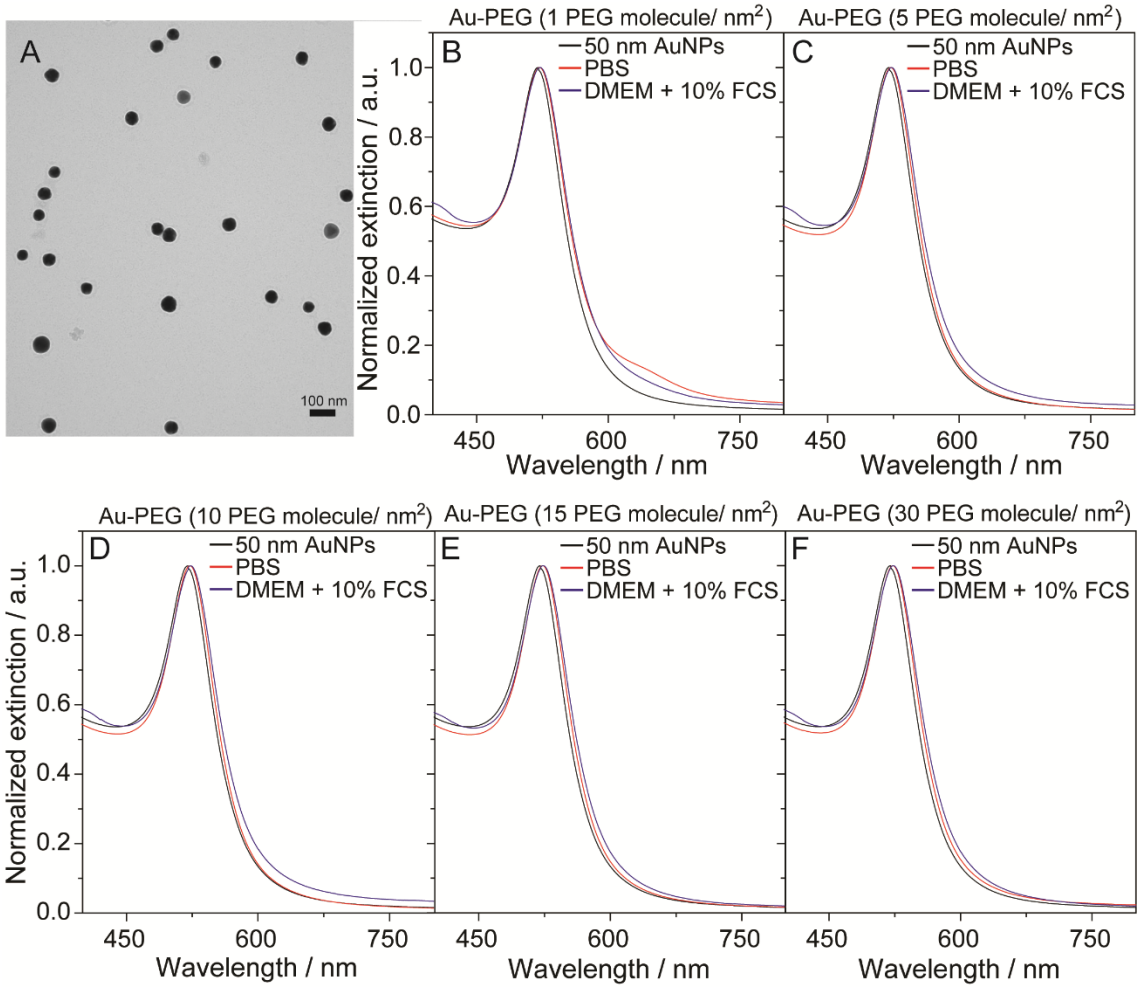

Figure S1. (A) Representative TEM micrograph with scale bar representing 100 nm of 50 nm AuNPs used as a core in this study. (B-F) UV-Vis spectra of PEGylated AuNPs in order to study of colloidal stability as a function of PEG grafting density, as indicated, in PBS buffer and 10 % FCS supplemented DMEM. UV-Vis spectra were normalized to unity at the extinction maximum.

Table S1. Zeta potential and hydrodynamic radius as function of PEG grafting density on AuNPs.

PEG molecules/nm^2	Zeta Potential[b] [mV] in PBS	Hydrodynamic radius[a] [nm] (PI)	
		PBS	*DMEM + 10 % FCS***
30	-19.2 ± 4.0	30.8 (49%)*	30.1 (41%)
15	-11.1 ± 7.8	30.8 (50%)*	30.5 (41%)
10	-17.8 ± 5.2	31.0 (61%)*	31.5 (53%)
5	-12.6 ± 4.0	31.1 (47%)*	31.3 (48%)
1	-5.3 ± 6.0	32.8 (39%)*	32.8 (47%)
0	-15.9 ± 1.7	20.7 (24%)	aggregation

[a] Mean hydrodynamic diameter obtained by depolarized dynamic light scattering (DDLS) at room temperature and at a scattering angle of 90°. DDLS measurements were carried out in triplicate. * Indicates a significant difference from Au as compared by a one-way ANOVA and Turkey's HDS test ($p< 0.05$). ** No significant difference between PBS-DMEM pairs as compared by a paired-sample t-test ($p<0.05$).

[b] Zeta-potentials were measured in 10 runs (mean ± SD).

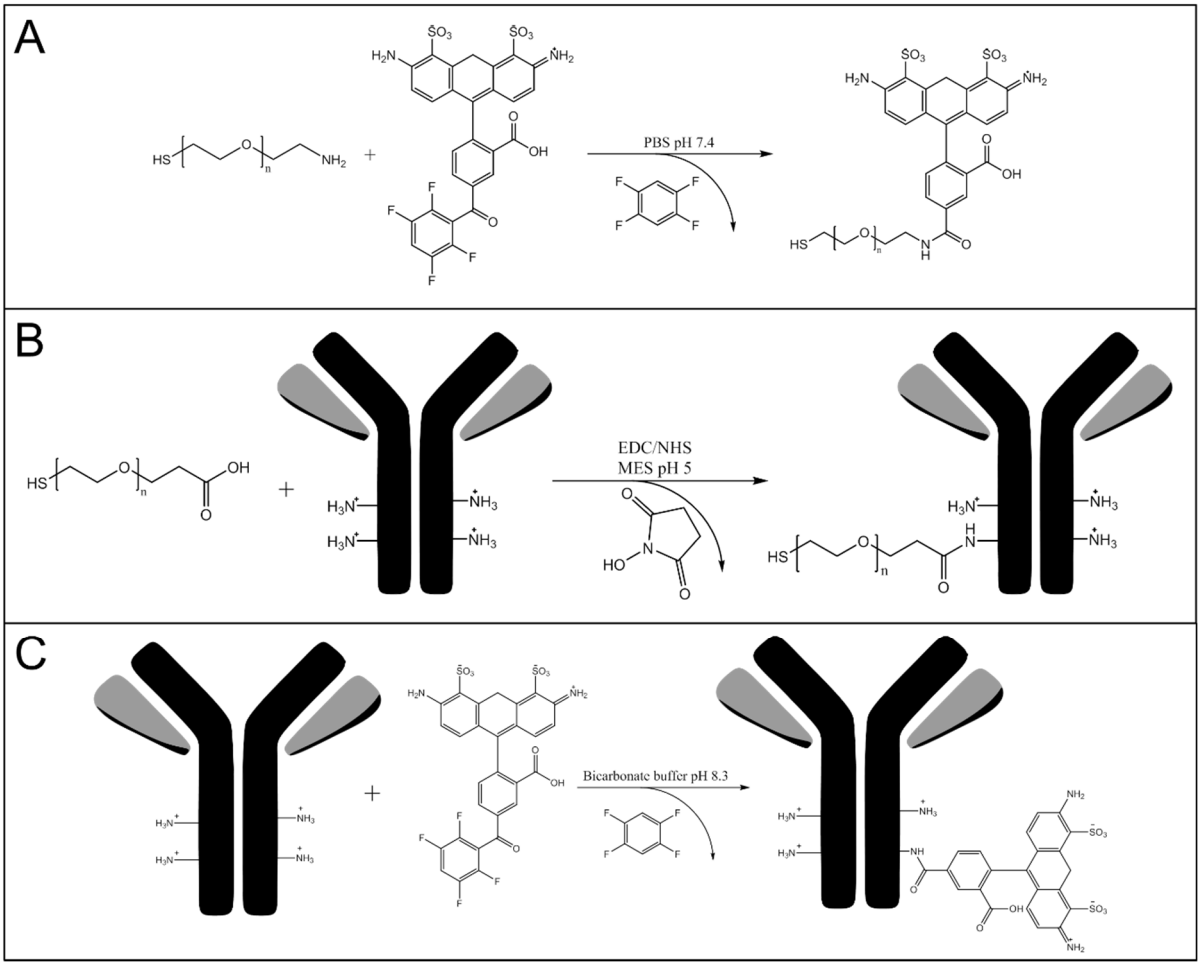

Figure S2. Labeling and conjugation reactions. (A) Alexa Fluor 488 conjugation to NH2-PEG-SH. (B) Trastuzumab conjugation to COOH-PEG-SH. (C) Alexa Fluor 488 conjugation to Trastuzumab.

We examined the possibility of PEG-AF488 displacement which could produce either the decrease of colloidal stability or the fluorescence decay. It is well-known that the binding of monothiol containing ligands to AuNPs can be unstable when exposed to heat, oxidizing agents or other thiolated small molecules such as glutathione or cysteine.[1–4] Therefore, we designed an experiment to compare the fluorescence decay when Au-PEGAF488 was incubated in PBS, supplemented DMEM, 1 mM EDTA solution, FACS buffer without or with EDTA. Moreover, the fluorescence decay was explored when AuNPs were put through dialysis or only incubation for 4 h. The **Figure S3** shows the fluorescence decay in the dialyzed AuNPs was lower than 20 % in all the case, except in 1 mM EDTA solution where the fluorescence decay was evident from the beginning and was more pronounced in the dialysed samples: 65 % in incubated AuNPs and 90 % in dialyzed AuNPs. Therefore, the presence of EDTA can have a negative impact in the fluorescence,[5] but this effect is reduced when EDTA is included in the FACS buffer. Therefore, the possible PEG displacement has a lower impact on our nanosystems.

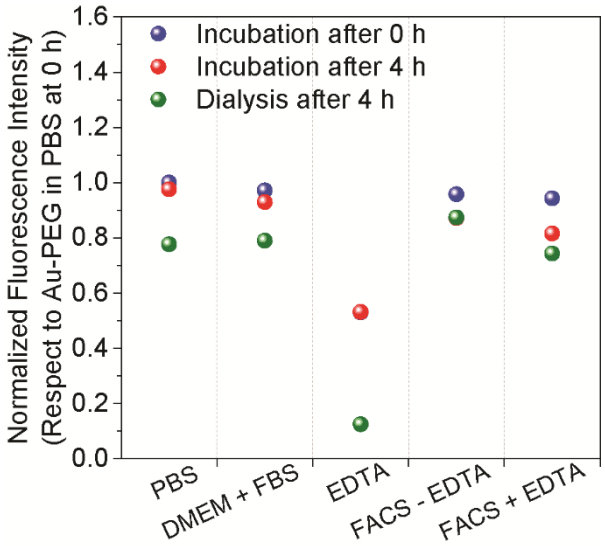

Figure S3. Displacement/Quenching of PEGAF488 from AuNPs (2 mM, which corresponds at 0.2 mg PEG) in PBS, 10 % FCS supplemented DMEM, 1 mM EDTA solution, FACS buffer without or with EDTA at room temperature for up to 4 h. The fluorescence intensity is normalized respect to the value from Au-PEGAF488 in PBS at 0 h.

Flow cytometry analysis. *Quantification of ERBB2 cell surface expression levels.* Quantum Simply Cellular anti-human IgG microbead kit (BLI816, Bangs Laboratories, Fishers, IN, USA) was adopted to quantify the level of ERBB2 expression on SK-BR-3, BT-474, and MDA-MD-231 cells. The experiments were conducted according to the manufacturer's protocols. Briefly, bead populations with increasing levels of Fc-specific capture Ab and cells were incubated with labeled Abs at saturating conditions (1 μg/condition) for 30 min at 4 °C. The labeled beads and cells were analyzed by flow cytometry (BD FACSCalibur Becton Dickinson, Allschwil, Switzerland). The Geo Mean of each bead population is recorded in the lot-specific QuickCal® template provided, where a regression curve is calculated associating the fluorescence value to the number of receptors in each bead population. The number of cell receptors is then extrapolated from the regression curve.

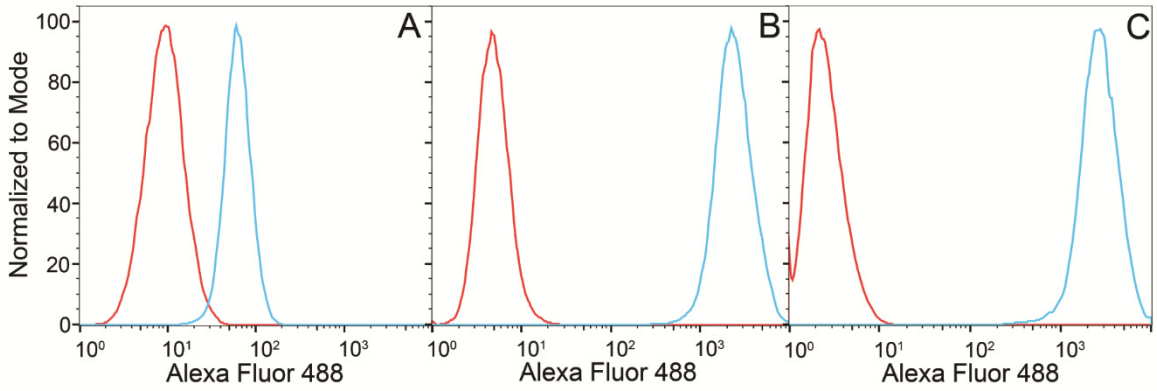

Breast Cancer cell line	ERBB2 receptors/unit area (μm²) [a,b]	Trastuzumab association[c]
SK-BR-3	9333	100 % (MFI ratio 1000)
BT-474	13779	100 % (MFI ratio 700)
MDA-MB-231	90	11 % (MFI ratio 6)

[a] Quantification of the level of expression of ERBB2 receptor was carried out through Simply Cellular ® anti-Mouse IgG standards (Bang Laboratories, Inc. Product 810). [b] Cell area (μm²): 375 ± 111 for SK-BR-3, 254 ± 76 for BT-474, and 1108 ± 343 for MDA-MD-231. [c] MFI ratio was normalized with negative control (cells alone) and the percentage of positive cells was estimated using FACS FlowJo software.

Figure S4. Levels of cell surface expression of ERBB2 in breast cancer cell lines. Flow cytometry analysis of MDA-MD-231 (A), BT-474 (B), SK-BR-3 (C) cells incubated with unlabeled anti-ERBB2 antibody TZB and labeled secondary antibody. Cells are shown in red-shaded histogram. Blue-shaded histograms show specific binding. The percentage of cell surface expression of ERBB2 in cells is given in Table. These data represent three independent experiments.

Trastuzumab (TZB)-conjugated AuNPs analysis by SDS-PAGE. SDS-PAGE analysis of TZB-conjugated AuNPs was carried out under reducing condition in polyacrylamide gels. Briefly, 80 μL of AuNPs (18 μg/mL) was incubated with 20 μL 15 mM β-mercaptoethanol (Sigma-Aldrich M6250) for 2 h. Then AuNPs samples were mixed with sample buffer (Tris-Cl/SDS, glycerol, 10 % SDS, bromophenol blue; Sigma-Aldrich). For reducing conditions, samples were boiled 5 min at 95 °C and centrifuged for 5 min. Samples and molecular weight standards were loaded onto the gels. Electrophoresis was carried out at a constant voltage of 120 V with 1X Tris-Glycine-SDS running buffer. Silver staining was used to detect proteins after electrophoretic separation.[6]

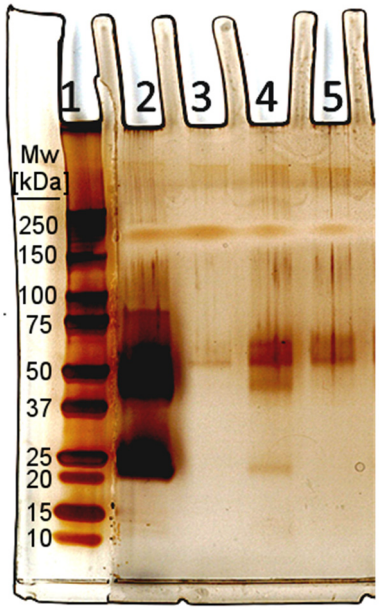

Figure S5. SDS-PAGE analysis of the supernatant obtained after incubating Antibody-conjugated AuNPs with β-mercaptoethanol for 2 h and boiling in the presence of SDS and β-mercaptoethanol. Lane 1, molecular weight marker. Lane 2, reduced TZB antibody (648 ng) as positive control. *Oriented Antibody-conjugated AuNPs:* Lane 3, Au-PEG-5TZB and Lane 4, Au-PEG-100TZB. *Non-oriented Antibody-conjugated AuNPs:* Lane 5, Au-PEG-100TZB.

Table S2. Number of AF488 molecules per AuNPs estimated through Fluorescence spectroscopy.

PEG:PEGAF488 ratio	AF488s/AuNP[b]
1:1	432 ± 144
1:100	1092 ± 457

[b]Fluorescence measured by means Victor plate reader with the filter set 560/615

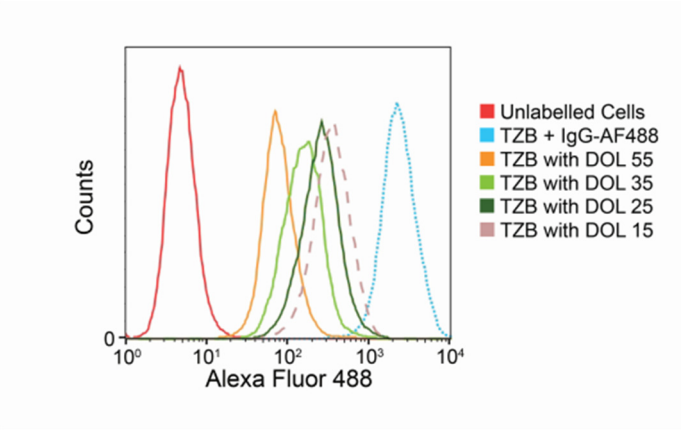

Figure S6. Effect of Alexa Fluor 488 labeling of the Trastuzumab (TZB) antibody on their specificity and binding characteristics to ERBB2 expressing cells. Flow cytometry after staining the BT-474 cell line with TZB at different degrees of AF488 labeling. The highest fluorescence enhancement in BT-474 was shown by TBZ with a degree of labeling (DOL) of 15 and 25, which corresponded an experimental DOL of 2.6 ± 0.6 and 3.8 ± 1.1, respectively. We selected labeled TZB with DOL of 25 in our study because it offered similar number of AF488 per AuNPs than the AuNPs functionalized with PEG:PEGAF488 with a ratio 1:1 (see Table 1 and Table S2).

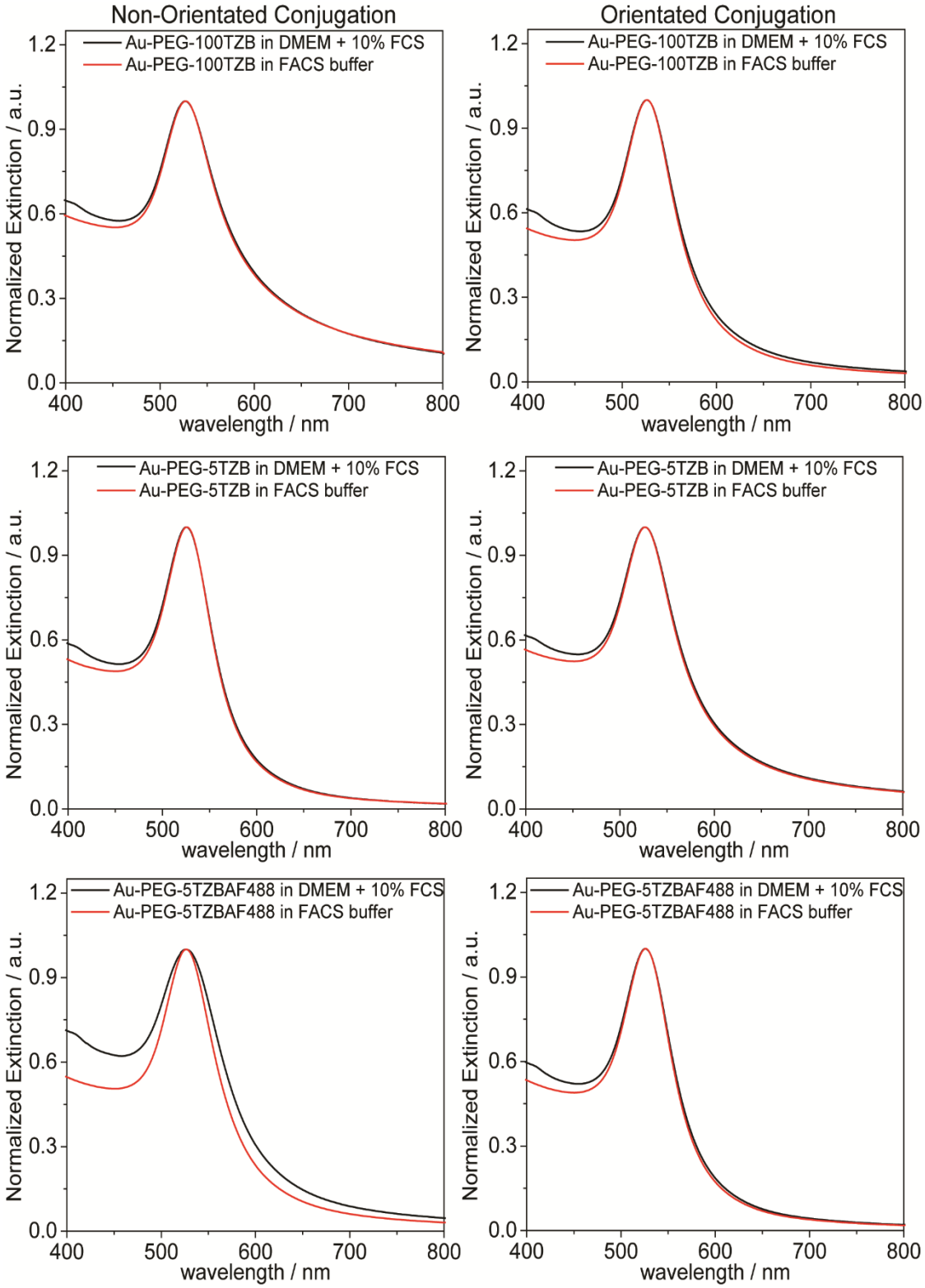
Non-Orientated Conjugation
Orientated Conjugation
Au-PEG-100TZB in DMEM + 10% FCS
Au-PEG-100TZB in FACS buffer
Au-PEG-5TZB in DMEM + 10% FCS
Au-PEG-5TZB in FACS buffer
Au-PEG-5TZBAF488 in DMEM + 10% FCS
Au-PEG-5TZBAF488 in FACS buffer
Normalized Extinction / a.u.
wavelength / nm
0.0
0.3
0.6
0.9
1.2
400
500
600
700
800

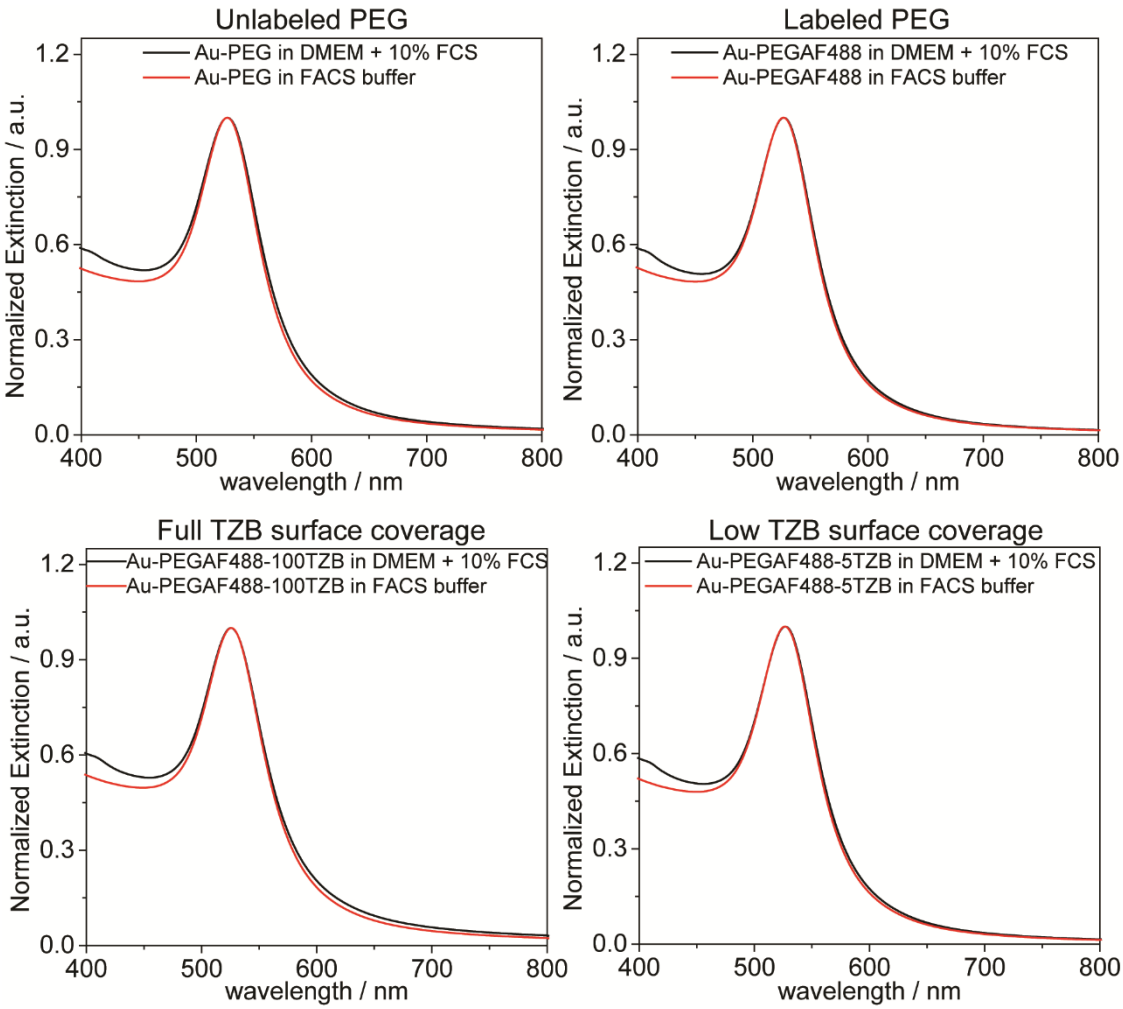

Figure S7. Colloidal stability study in 10 % FCS supplemented DMEM and FACS buffer using UV-Vis spectroscopy. Extinction spectra were normalized to unity at the extinction maximum.

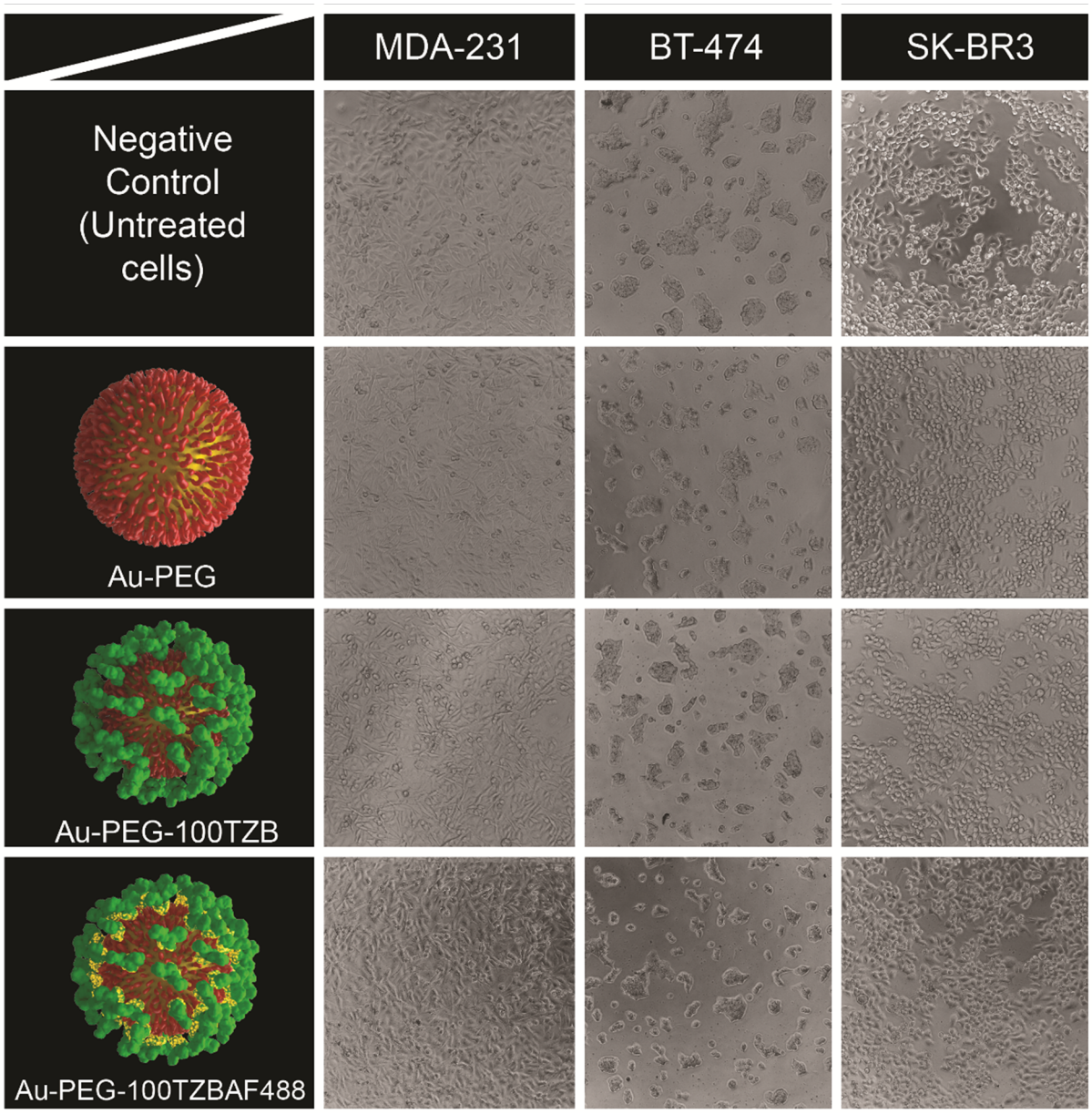

Figure S8. Phase contrast images of MDA-MB-231, BT-474 and SK-BR3 breast cancer cell lines after incubation with (from top to bottom) no particles (control), Au-PEG, Au-PEG-100TZB, Au-PEG-100TZBAF488, Au-PEGAF488, Au-PEGAF488-5TZB, Au-PEGAF488-100TZB and 1 % Triton X-100 (Positive control).

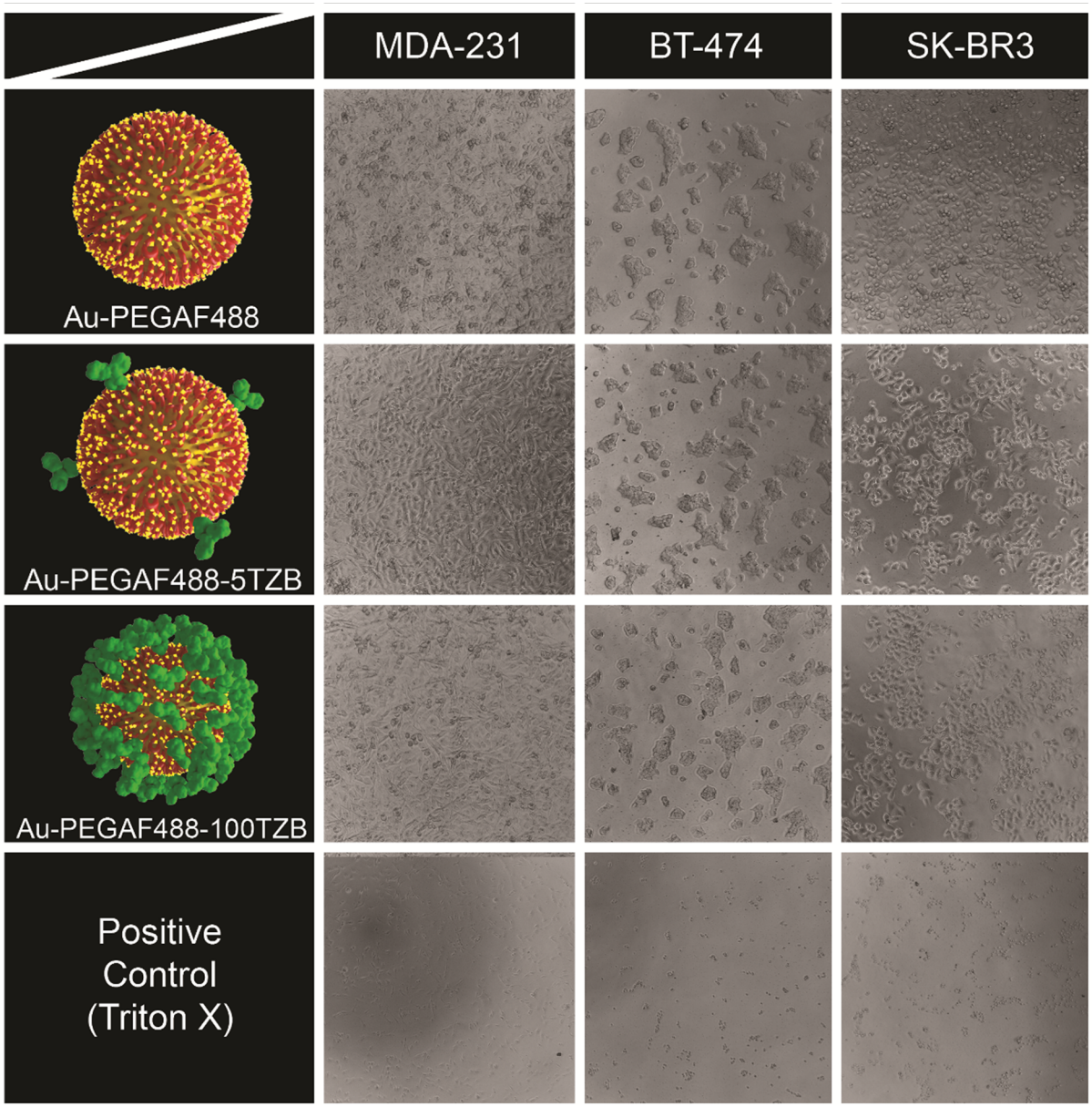

Figure S8 (continuation). Phase contrast images of MDA-MB-231, BT-474 and SK-BR3 breast cancer cell lines after incubation with (from top to bottom) no particles (control), Au-PEG, Au-PEG-100TZB, Au-PEG-100TZBAF488, Au-PEGAF488, Au-PEGAF488-5TZB, Au-PEGAF488-100TZB and 1 % Triton X-100 (Positive control).

Cytotoxicity assay. The cytotoxicity of labeled and unlabeled PEGylated AuNPs sets against all cell lines was investigated by an MTT assay. Cells re-suspended in fresh cell culture medium were seeded into 96-well plates at 2×10^4 cells per well and cultured for 24 h in 5 % CO_2 atmosphere at 37 °C. Then, the medium was discarded and replaced with fresh medium containing AuNPs at the final concentration of 40 μg/mL (100 μL). After 24 h incubation, medium was removed and cells were washed 3 times with PBS (3x 100 μL). Afterwards, 3-(4,5-dimethylthiazol-2-yl)-2,5-diphenyltetrazolium bromide (MTT; Sigma-Aldrich) viability assay was performed according to the standard protocol.[7] Briefly, 5 mg/mL MTT (10 μL) solution was added to each well. After 4 h incubation, MTT solution was aspirated and 100 μL of DMSO was added to each well to dissolve the crystals. After 30 min incubation with agitation, absorption at 570 nm was measured with a Victor™ X3 2030 multi-label reader (Perkin Elmer, Schwerzenbach, Switzerland). Untreated cells were used as negative control (100 % viability) and 0.1 % Triton X-100-treated cells were used as positive control (cell lysis, 0% viability). Sample mean values were compared with a one-way ANOVA and Tukey's honest significant difference (HSD) test ($p < 0.05$).

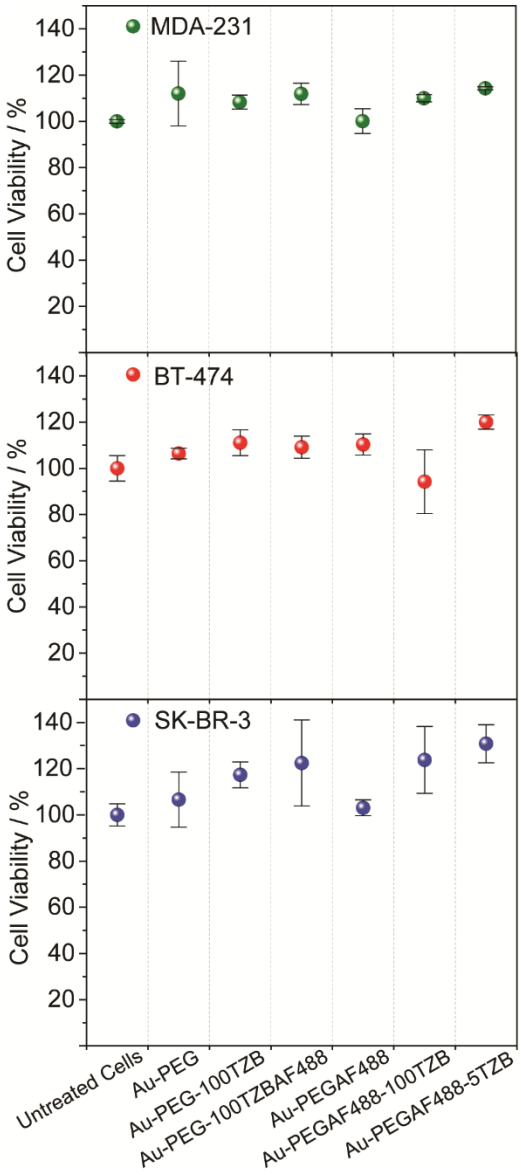

Figure S9. The viability of MDA-MD-231 (green), BT-474 (red), and SK-BR3 (blue) cell lines incubated for 24 h with the indicated NPs, was determined by MTT assay (mean ± SD). Values were significant when compared to cells treated with medium only (one-way Turkey post-hoc ANOVA, $*p < 0.05$). Triton X-100 at 1 % V/V was used as the control for 0% viability.

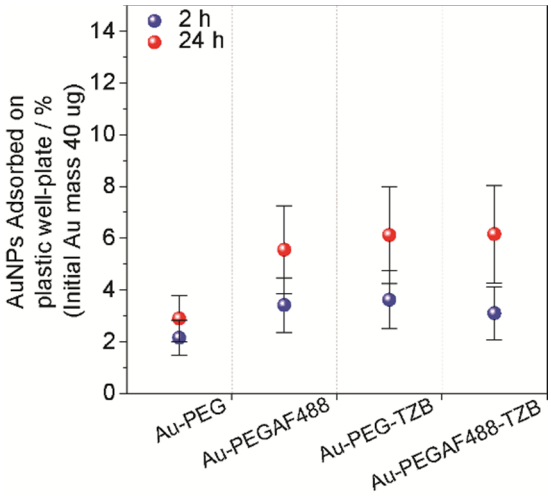

Figure S10. ICP-OES analysis of Au-PEG, Au-PEGAF488, Au-PEG-TZB and Au-PEGAF488-TZB samples on plastic well plates after incubating for 2 and 24 h at 40 μg/mL in complete media with no cells.

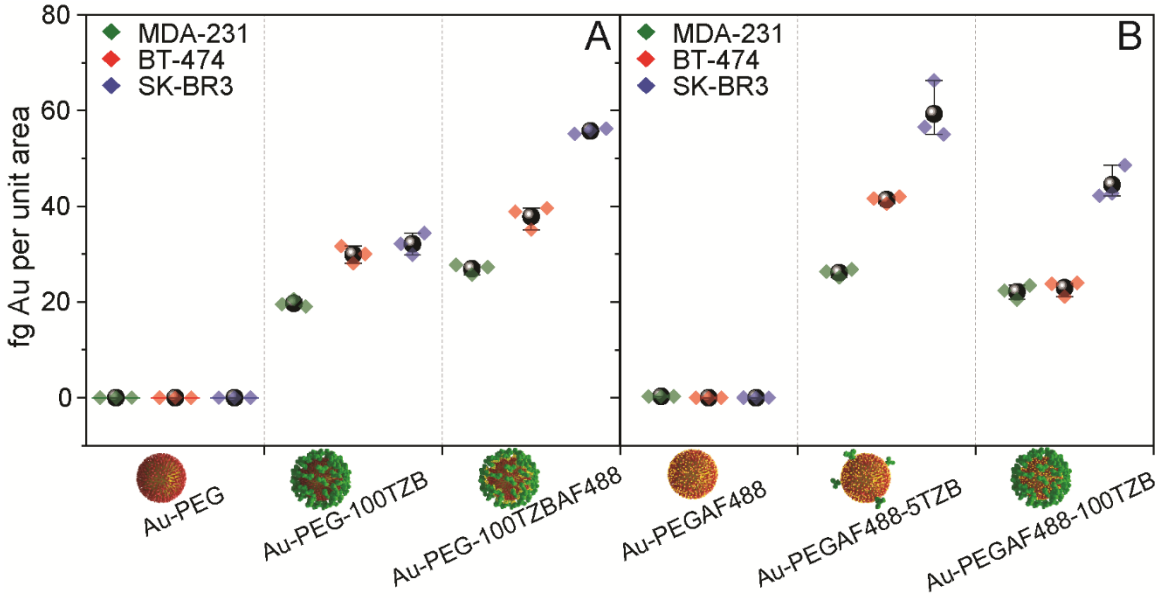

Figure S11. Quantification of specific cellular binding of unlabeled PEGylated AuNPs (A) and AF488-labelled PEGylated multifunctional AuNPs (B) by ICP-OES in three breast cancer cell lines: MDA-MD-231 (green), BT-474 (red), and SK-BR-3 (blue). The cells were incubated with 40 μg/mL NPs for 24 h. Each NP type was measured in triplicate (semi-transparent diamonds). The black spheres and lines indicate the mean and SD respectively. Split-plot ANOVA with Huynh-Feldt correction for non-sphericity and Bonferroni's post hoc test were performed to evaluate non-statistically significant differences with Au-PEG and Au-PEGAF488 (* $p < 0.05$), respectively

Laser scanning microscopy (LSM) and enhanced dark-field optical microscopy with high-resolution hyperspectral imaging. Cells were seeded onto fibronectin-coated 8-well culture slides (Thermo Fisher) and exposed to AuNPs at 40 μg/mL for 24 h at 37 °C in 5 % CO_2. After incubation, wells were washed twice with PBS, and cells fixed with 4 % paraformaldehyde (PFA) in PBS for 15 min at room temperature. Cells were then permeabilized with 0.3 % Triton X-100 in PBS for 15 min and blocked with blocking buffer (0.05 % BSA, 5 % Donkey serum, 0.1 % Triton X-100 in PBS). Over a period of 2 h, the actin cytoskeleton was stained with AlexaFluor® 546 phalloidin (Molecular Probes, Thermo Fischer) at 132 nM (6.6 μM stock dye solution diluted 1:50 in blocking buffer), and cell nuclei were labeled with 4',6-diamidin-2-phenylindol (DAPI; Molecular Probes, Life technologies) at 1 μg/mL in blocking buffer. Samples were then mounted in Glycergel mounting medium (Dako Schweiz Baar, Switzerland) and coverslipped. An inverted Zeiss confocal laser scanning microscope 710 (LSM, Axio Observer.Z1) (Carl Zeiss, Jena, Germany) was used to visualize the samples. Image processing was conducted using Fiji Image J software.

Hyperspectral images were acquired on a CytoViva hyperspectral microscope (CytoViva, Inc., Auburn, AL, USA) outfitted with a Dolan-Jenner DC-950 light source, UPL Fluorite 100× objective, and SPECIM V10E imaging spectrograph with a PCO pixelfly detector. 1 mg/mL Trastuzumab in a 1:50 dilution and a 2 mg/mL fluorescent secondary antibody in a 1:100 dilution (Alexa Fluor 488 goat anti-human IgG, Life Technologies) were used as a positive control to visualize ERBB2. As a negative control, wells were exposed to media only (no cells) and cells only.

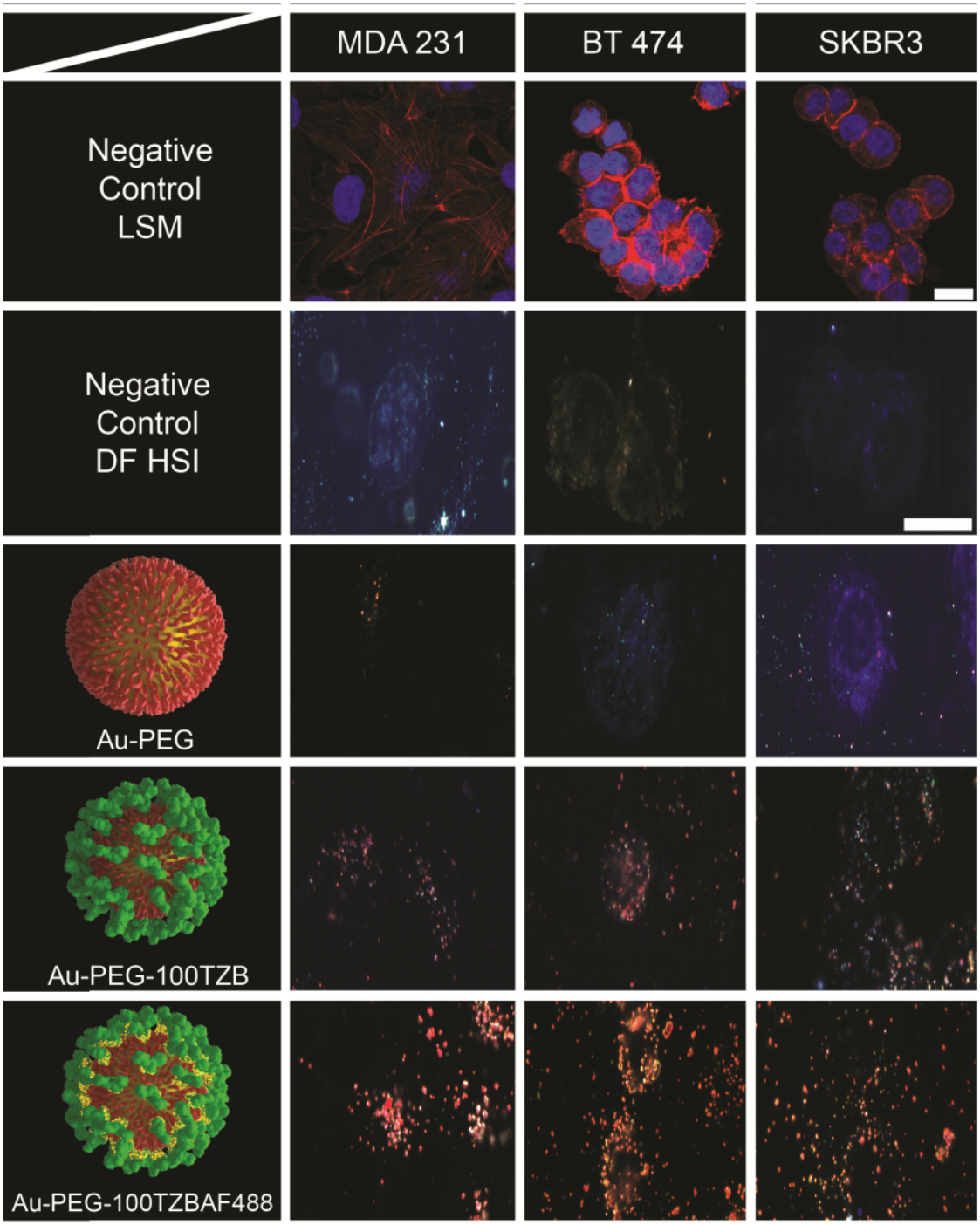
MDA 231
BT 474
SKBR3
Negative Control LSM
Negative Control DF HSI
Au-PEG
Au-PEG-100TZB
Au-PEG-100TZBAF488

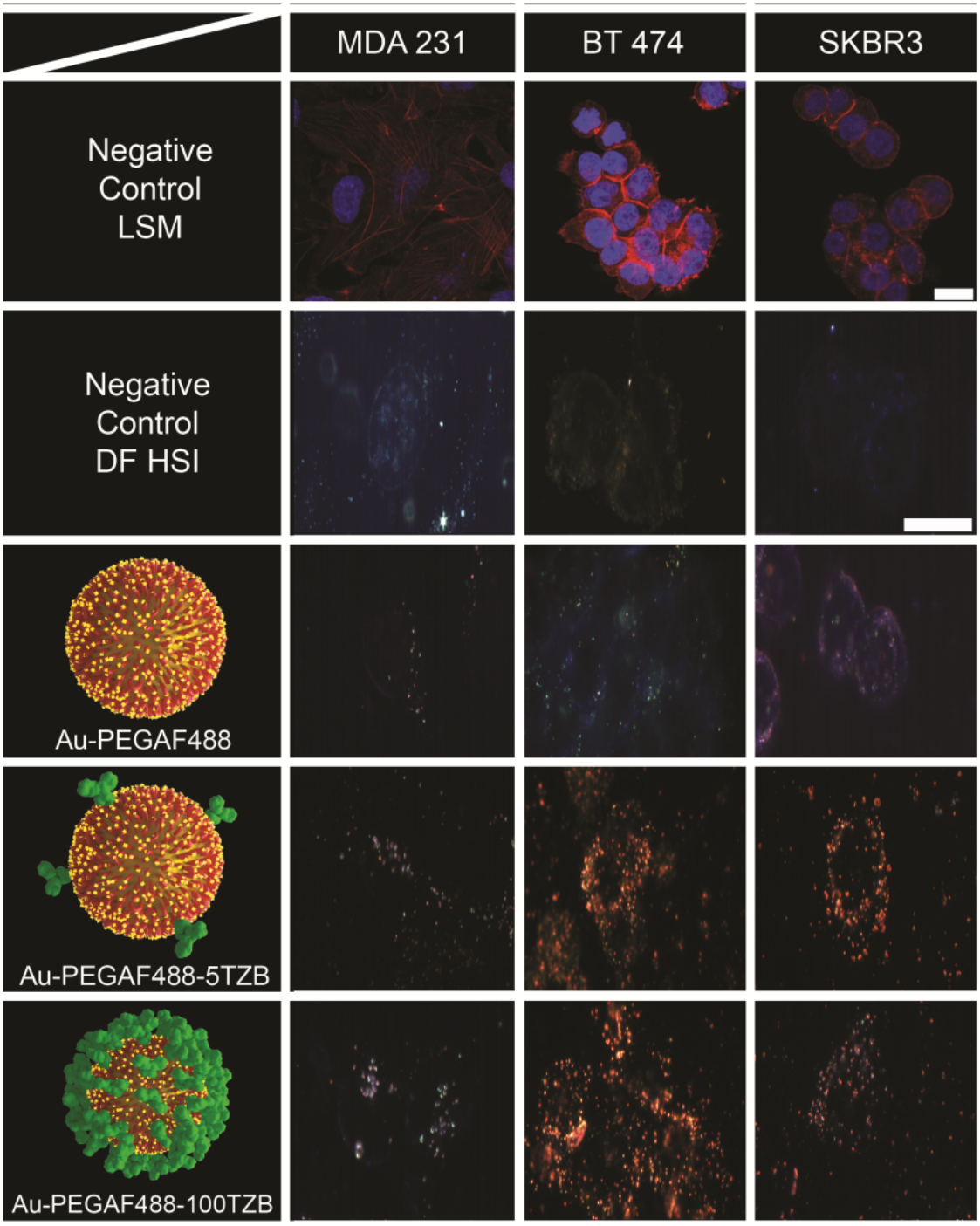

Figure S12. Hyperspectral imaging combined with dark-field light microscopy of MDA-MB-231, BT-474 and SK-BR-3 after incubation for 24 h with the multifunctional AuNPs (40 µg/mL) before undergoing fixation, embedding, and imaging. Scale bar, either laser scanning images (shorter) or hyperspectral images (longer), corresponds to 10 µm.

DDLS theory

Light scattering measurements were acquired as described in the "Material and Methods" section into the main manuscript of the text. The field auto-correlation functions were obtained via the Siegert relation:

$$g_1(t) = \sqrt{g_2(t) - 1} \quad (1)$$

where $g_2(t)$ is the intensity auto-correlation function constructed from the temporal fluctuations of the depolarized component of the scattered intensity.

At sufficiently short times, the decay of the correlation function is proportional to time:[8]

$$g_1(t) \cong 1 - \langle \Gamma \rangle t \quad (2)$$

where $\langle \Gamma \rangle = \frac{k_B T}{\pi \eta} \left(\frac{6 \langle r^3 \rangle}{8 \langle r^6 \rangle} + \frac{q^2}{6} \frac{\langle r^5 \rangle}{\langle r^6 \rangle} \right)$, (3)

is the relaxation rate and

$$\langle r^n \rangle = \int_0^\infty P(r) r^n dr \quad (4)$$

is the n^{th} raw moment of P(r), which stands for the number-averaged size distribution of the hydrodynamic radius. When the polydispersity is moderate: $\left\langle \frac{r^6}{r^5} \right\rangle \cong \sqrt[3]{\left\langle \frac{r^6}{r^3} \right\rangle} \cong \langle r \rangle$ and

$$\langle \Gamma \rangle = \frac{k_B T}{\pi \eta} \left(\frac{6}{8} \frac{1}{\langle r \rangle^3} + \frac{q^2}{6} \frac{1}{\langle r \rangle} \right). \quad (5)$$

$\langle \Gamma \rangle$ is estimated from experiments by fitting the early decay of $g_1(t)$ against a linear function, and $\langle r \rangle$ is quantified via Equation 5.[9]

REFERENCES

(1) Yook, S.; Lu, Y.; Jeong, J. J.; Cai, Z.; Tong, L.; Alwarda, R.; Pignol, J.-P.; Winnik, M. A.; Reilly, R. M. Stability and Biodistribution of Thiol-Functionalized and 177Lu-Labeled Metal Chelating Polymers Bound to Gold Nanoparticles. *Biomacromolecules* **2016**, *17*, 1292–1302.

(2) Kang, J. S.; Taton, T. A. Oligothiol Graft-Copolymer Coatings Stabilize Gold Nanoparticles against Harsh Experimental Conditions. *Langmuir* **2012**, *28*, 16751–16760.

(3) Guo, R.; Song, Y.; Wang, G.; Murray, R. W. Does Core Size Matter in the Kinetics of Ligand Exchanges of Monolayer-Protected Au Clusters? *J. Am. Chem. Soc.* **2005**, *127*, 2752–2757.

(4) Zhang, G.; Yang, Z.; Lu, W.; Zhang, R.; Huang, Q.; Tian, M.; Li, L.; Liang, D.; Li, C. Influence of Anchoring Ligands and Particle Size on the Colloidal Stability and in Vivo Biodistribution of Polyethylene Glycol-Coated Gold Nanoparticles in Tumor-Xenografted Mice. *Biomaterials* **2009**, *30*, 1928–1936.

(5) Lee, T. Y.; Suh, J. Target-Selective Peptide-Cleaving Catalysts as a New Paradigm in Drug Design. *Chem. Soc. Rev.* **2009**, *38*, 1949–1957.

(6) Chevallet, M.; Luche, S.; Rabilloud, T. Silver Staining of Proteins in Polyacrylamide Gels. *Nat. Protoc.* **2006**, *1*, 1852–1858.

(7) Mosmann, T. Rapid Colorimetric Assay for Cellular Growth and Survival: Application to Proliferation and Cytotoxicity Assays. *J. Immunol. Methods* **1983**, *65*, 55–63.

(8) Geers, C.; Rodriguez-Lorenzo, L.; Andreas Urban, D.; Kinnear, C.; Petri-Fink, A.; Balog, S. A New Angle on Dynamic Depolarized Light Scattering: Number-Averaged Size Distribution of Nanoparticles in Focus. *Nanoscale* **2016**, *8*, 15813–15821.

(9) Balog, S.; Rodriguez-Lorenzo, L.; Monnier, C. A.; Obiols-Rabasa, M.; Rothen-Rutishauser, B.; Schurtenberger, P.; Petri-Fink, A. Characterizing Nanoparticles in Complex Biological Media and Physiological Fluids with Depolarized Dynamic Light Scattering. *Nanoscale* **2015**, *7*, 5991–5997.